Oxygen-Deficient Line Defects in an Ultrathin Aluminum Oxide Film

M. Schmid,[1] M. Shishkin,[2] G. Kresse,[2,*] E. Napetschnig,[1] P. Varga,[1] M. Kulawik,[3] N. Nilius,[3] H.-P. Rust,[3] and H.-J. Freund[3]

[1]*Institut für Allgemeine Physik, Technische Universität Wien, A 1040 Wien, Austria*
[2]*Institut für Materialphysik and Centre for Computational Materials Science, Universität Wien, A 1090 Wien, Austria*
[3]*Fritz-Haber Institut der MPG, Faradayweg 4-6, D 14195 Berlin, Germany*
(Received 31 January 2006; published 24 July 2006)

A model for the straight antiphase domain boundary of the ultrathin aluminum oxide film on the NiAl(110) substrate is derived from scanning tunneling microscopy measurements and density-functional theory calculations. Although the local bonding environment of the perfect film is maintained, the structure is oxygen deficient and possesses a favorable adsorption site. The domain boundary exhibits a downwards band bending and three characteristic unoccupied electronic states, in excellent agreement with scanning tunneling spectroscopy measurements.

DOI: 10.1103/PhysRevLett.97.046101 PACS numbers: 68.35.Bs, 68.37.Ef, 68.43.Bc, 68.47.Gh

The study of aluminum oxides is motivated by fundamental scientific interest as well as by their technological relevance, e.g., as support in heterogenous catalysis. An important role in enhancing catalytic reactions is believed to be played by structural defects, in particular, oxygen vacancies, which act as adsorption centers for molecules or metallic clusters [1,2]. Atomic-scale studies of such vacancies are exceedingly difficult, since insulating bulk oxides cannot be probed by many experimental techniques, such as scanning tunneling microscopy (STM). A way to circumvent this problem is to study ultrathin oxide films grown on conducting substrates. Because of the structural complexity of these films, the microscopic interpretation of experimental data remains a challenge. Here we demonstrate that straight antiphase domain boundaries (see Refs. [3,4]) of ultrathin alumina films on the NiAl(110) substrate are oxygen deficient and possess a favorable adsorption site for electronegative species. We will argue that these sites behave in many respects like regularly arranged oxygen vacancies, albeit with a much reduced oxygen addition and removal energy than at other sites.

The basis for the present work has been laid recently by solving the long standing puzzle of the structure of the ultrathin aluminum oxide film on NiAl(110) [3–9]. The surface consists of oxygen atoms (named O_s) arranged in squares and triangles, and aluminum atoms (Al_s) in between, only slightly below the O_s layer [Fig. 1(e)]. The oxide film also contains another oxygen layer (O_i) and the Al_i layer at the interface with the substrate. The arrangement of the atoms in the oxide has $p2gg$ planar symmetry with four glide planes, which explains its almost perfectly rectangular unit cell. The stoichiometry of the film is $Al_4O_6Al_6O_7$ in contrast to the usual Al_2O_3 stoichiometry. The reason for this unusual stoichiometry is that the interfacial Al atoms (Al_i) bind strongly to the substrate and donate only two electrons to the film (Al^{+2}). Thus, despite its unusual stoichiometry, the film is autocompensated, with a band gap in the surface layer close to that of bulk Al_2O_3. The registry of substrate and oxide is enforced by the Al_i atoms, which are mostly above the Ni rows, thereby anchoring the film. This row matching leads to stress in the oxide film along the $[1\bar{1}0]$ direction of NiAl. The observed deformation of the otherwise rectangular unit cell into a parallelogram [6] indicates that this stress is compressive, and we will argue that this stress is also the reason for the incorporation of line defects in the oxide (often referred to as antiphase domain boundaries) [3]. The determination of their structure is the main achievement of the present work.

The STM measurements were obtained in Vienna using an ultrahigh vacuum (UHV) room-temperature (RT) and a low-temperature (LT) STM system at 80 K [9] and in Berlin with a LT UHV instrument operated at 5 K [10]. The ultrathin alumina layer was prepared by cleaning the NiAl(110) surface, followed by cycles of oxidation at 500–550 K and subsequent annealing to 1000–1100 K [5]. This oxide does not contain any Ni [5,11]. Structural optimization and calculations of the energetics have been performed using the density-functional theory (DFT) package VASP [12]. A gradient-corrected functional was used for the treatment of exchange-correlation effects [13], and wave functions were expanded in plane waves with a cutoff energy of 250 eV. When more accurate one-electron energies were required (density of states) the HSE03 hybrid functional with 25% screened exchange and 75% DFT exchange was used [14], as recently implemented in the VASP code [15]. Electron-ion interactions were described by the projector augmented-wave method [16] in the implementation of Kresse and Joubert [17]. The computational cell includes a slab of 4 NiAl layers, and the Brillouin zone was sampled at the Γ point (for the electronic density of states, two k points were used).

Combined results of STM measurements and DFT simulations of the antiphase domain boundary structure are presented in Fig. 1. The model is based on the experimental STM images shown in Figs. 1(a)–1(c). Crucial for the

 © 2006 The American Physical Society

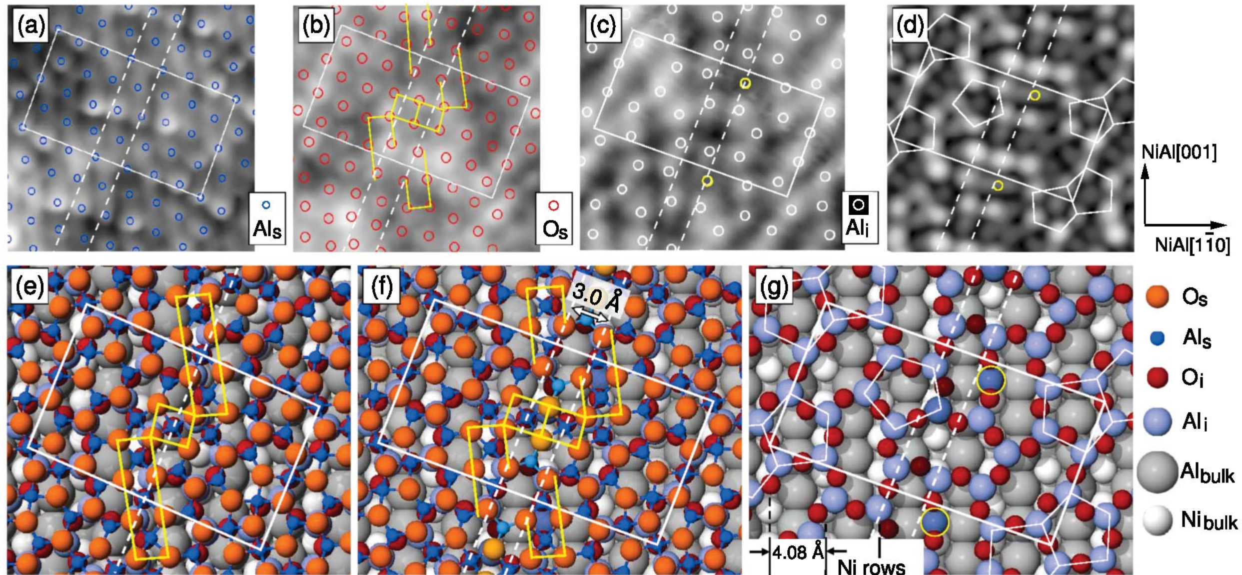

FIG. 1 (color). (a)–(d) Experimental and theoretical STM images of the domain boundary: (a) 80 K, −570 mV, 0.34 nA; (b) RT, −0.4 mV, 0.5 nA; (c) 5 K, −250 mV, 0.5 nA; (d) simulation based on the Tersoff-Hamann approach. Models of (e) the perfect film and (f) the domain boundary. In (g) only the oxygen (O_i) and aluminum (Al_i) atoms close to the NiAl substrate are shown for the domain boundary model. Calculated atom positions are also shown as circles in the STM images. The unit cell used in the simulation is denoted by the white rectangle, and the dashed lines show where extra atoms are inserted in the boundary between two oxide domains. Pentagons in the interface and some characteristic units in the surface are highlighted by white and yellow lines, respectively.

construction of the model is that one can image—with a certain caveat as demonstrated below—three out of four atomic layers. In combination with the building principles established in our previous work [9] the structure of the antiphase domain boundary can be determined almost unambiguously.

Figure 1(a) was taken at low temperature (80 K) under conditions where the topmost Al atoms (Al_s) are imaged [9]. The almost perfect hexagonal arrangement of these atoms remains conserved at the domain boundary [3]. The second image [Fig. 1(b)], taken at room temperature and very low bias voltage, shows the surface oxygen atoms (O_s). The final image [Fig. 1(c)], taken at LT again but now with a different tip state than Fig. 1(a), shows only those surface oxygen atoms that have an Al_i atom below. Here the density of states is scanned at rather large distances from the surface. Since the Al_i atoms enhance the tunneling probability of metallic NiAl states into the vacuum, and it is these states one now sees, the Al_i atoms are indirectly probed [9]. Mind, however, that the Al_i atoms are only visible if an O_s atom is located above them (see below).

Construction of the model is now straightforward. The cell of the original oxide film [Fig. 1(e)] is split in the middle along the dashed line and the two pieces are moved apart by 3.0 Å. This value can be deduced from the STM experiments by comparison of the unperturbed cells and the domain boundary. In the surface layer, aluminum atoms and oxygen atoms are added according to the experimental STM images [Figs. 1(a) and 1(b), respectively]. This is done by duplicating the atoms along the dashed line and inserting additional atoms, marked by slightly different colors in Figs. 1(f) and 1(g). According to the building rules of the film, an interfacial oxygen atom (O_i) is located below each Al_s atom [9]. Finally, Al_i atoms are added at the bright positions shown in Fig. 1(c). This, however, violates an important principle observed for the oxide film: each O_i atom should bind to two Al_i atoms. The coordination fault can be cured by adding an aluminum atom at the position indicated by the yellow circle in Figs. 1(c), 1(d), and 1(g).

Assuming similar bond lengths in the domain boundary as in the unperturbed oxide film, inserting the extra atoms needs $\approx$3.0 Å space in the direction of the long side of the alumina unit cell [Fig. 1(f)], in agreement with the experimental value. Since the domain boundary cell bridges one more substrate Ni row than the unperturbed cell [Fig. 1(e)], its long side is $4.08\ \text{Å}/\cos 24° = 4.47$ Å longer [Fig. 1(g)]. The extra space of $\approx$1.5 Å allows the film to reduce its compressive stress.

To model the interface, a supercell was constructed using a

$$\begin{pmatrix} 5 & -3 \\ 1 & 4 \end{pmatrix}$$

NiAl cell with 23 elementary surface cells and adjusting this substrate lattice to be commensurate with the oxide cell containing the domain boundary. The substrate is slightly strained and was therefore not allowed to relax. The STM image [Fig. 1(d)], calculated using the Tersoff-Hamann approach [18], closely resembles the experimental results. Depending on the distance at which the isosur-

face is evaluated, the image either corresponds to the experimental STM images at low bias voltages [Fig. 1(b)] or at higher voltages [Fig. 1(c)]. Here a value was adopted yielding images intermediate to the two experimental cases (bright spots correspond to a distance of 2.5 Å above the core of the O_s atoms). Clearly, the STM simulation does not show the presence of the interface Al atom marked by a yellow circle, in agreement with the experimental images. Thus a direct experimental proof or disproof of its existence cannot be given. To deal with this uncertainty, we performed DFT calculations and determined the formation energy of vacancies or additional interstitials (see below) as

$$\Delta\gamma = (E_{\mathrm{domain/def}} - E_{\mathrm{domain}} \pm N_{\mathrm{Al}}\mu_{\mathrm{Al}} \pm N_{\mathrm{O}}\mu_{\mathrm{O}})/\mathrm{area},$$

where $E_{\mathrm{domain/def}}$ and E_{domain} are the total energies of the cell with a defect (the cell with an Al vacancy in this case) and the original domain boundary cell [Fig. 1(f)], respectively. N_{O}, N_{Al} and μ_{Al}, μ_{O} are the number of added or removed oxygen and aluminum atoms in the oxide film and the corresponding chemical potentials. According to Ref. [19], the chemical potential of an aluminum atom is typically 1 eV more favorable in NiAl than in bulk fcc aluminum, whereas for oxygen we use an oxygen molecule as reference. Removal of the Al_i atom discussed above is found to be very unfavorable (2.2 eV with respect to NiAl), strongly indicating the presence of this atom.

The stoichiometry of the film including an antiphase domain boundary is thus $(\mathrm{NiAl})_{23}\mathrm{Al}_{19}\mathrm{O}_{28}\mathrm{Al}_{28}\mathrm{O}_{32}$. As the valence of Al_i and Al_s atoms is +2 and +3, respectively, the film is not autocompensated and lacks one oxygen atom $(2 \times 19 + 3 \times 28 - 2 \times 60 = +2)$. Usually an oxygen deficiency implies that two electrons occupy electronic defect states with Al $3p$ character close to the conduction band edge (F center), but here this is not the case. The partial density of states (PDOS) of the surface Al and O atoms has been calculated [Figs. 2(a) and 2(b)] using a conventional gradient-corrected density functional (GGA, Ref. [13]) and the HSE03 hybrid functional [14]. The results are qualitatively similar for both cases, and we concentrate here on the hybrid density-functional results, which better account for the gap in bulk $\mathrm{Al}_2\mathrm{O}_3$ ($E_g^{\mathrm{GGA}} = 6.3$ eV, $E_g^{\mathrm{HSE03}} = 8.0$ eV, $E_g^{\mathrm{exp}} \approx 9.5$ eV) and in the thin film ($E_g^{\mathrm{GGA}} \approx 4.0$ eV, $E_g^{\mathrm{HSE03}} \approx 6.3$ eV, $E_g^{\mathrm{exp}} \approx 6.7$ eV; see Ref. [20]). The calculated PDOS of the perfect oxide [Fig. 2(a)] shows that the Fermi level is pinned in the midpoint between the conduction band and valence band edges. The domain boundary [Fig. 2(b)] reveals two states located below the conduction band edge of the perfect film (2.3 and 2.9 eV) and a pronounced third peak at +3.9 eV. From the previous arguments, we might have expected an even stronger shift of the Fermi level all the way up to the first defect state. The shift is, however, smaller, since two electrons are transferred to the NiAl support; i.e., the situation is best described as $(\mathrm{NiAl})^{2-}_{\mathrm{substr}}(\mathrm{Al}_{19}\mathrm{O}_{28}\mathrm{Al}_{28}\mathrm{O}_{32})^{2+}$, and the defect states remain unoccupied. To counterbalance the electron transfer and in agreement with the formal charges, a local band bending occurs at the defect, causing a local downshift of the valence and conduction bands by roughly 1.0 eV.

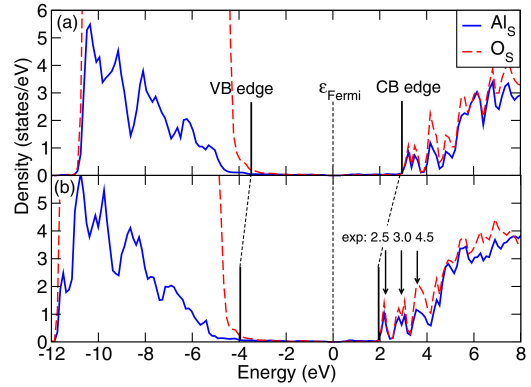

FIG. 2 (color online). PDOS of (a) the perfect oxide and (b) the cell containing a domain boundary, calculated using the hybrid functional. Three peaks are highlighted by the vertical arrows, and the conduction band (CB) and valence band (VB) edges are marked. The energies are aligned at the Fermi level.

We note that the energies of the defect states are in close agreement with recent scanning tunneling spectroscopy experiments showing empty conduction band states at +2.5, +3.0, and +4.5 eV [4]. In the experiment it was observed that the first of these defect states was localized at the domain boundary, whereas the second one was visualized as a double stripe centered at the domain boundary. The size of our supercell is too small to account for all details; in particular, the lateral extent of the second defect state approaches that of our cell. The first state located at +2.3 eV, however, is localized between the two aluminums Al1 and Al2 in Fig. 3(a) (light blue). It is tempting to assume that this particular site is a favorable adsorption center: as already mentioned, the stoichiometry of the domain boundary relates to an oxygen deficiency. Adsorption of an electronegative atom at this site should be very favorable, since it will take up the two electrons from the

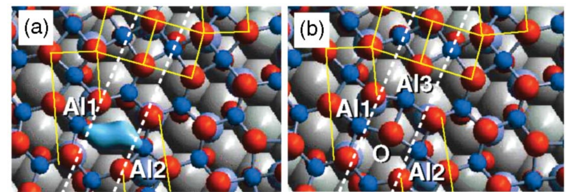

FIG. 3 (color). (a) Isosurface (light blue) of the density distribution corresponding to the states in the vicinity of the first peak in the conduction band. The Al atoms (dark blue), on which the lowest defect state is localized, are marked as Al1 and Al2. For guidance, the domain boundary is indicated by the dashed white lines and the same features as in Fig. 1(f) are highlighted by yellow lines. (b) Optimized structure with an additional O atom forming bonds with the atoms Al1, Al2, and Al3.

NiAl reservoir. Furthermore, the local geometry is such that additional atoms are easily incorporated.

As a first test we have considered the adsorption of oxygen atoms and found that upon adsorption and relaxation the additional O atom forms chemical bonds with the three neighboring Al atoms, leaving largely intact the remaining bond topology [Fig. 3(b)]. The binding of this O atom is quite favorable with a binding energy of -3.61 eV (with respect to O_2), and the defect states vanish upon adsorption. This leaves the question of why oxygen was not included during film growth at this particular site. For comparison, the energy required for removal of other surface O atoms has been determined for the perfect film [Fig. 1(e)]. The range of calculated values (5.5–6.5 eV) shows that formation of any O vacancy in the film is significantly less favorable than from the "defect" site in our present model. Since the O atom is not observed in STM images, the preparation conditions must be sufficiently reducing so that no oxygen can be trapped at the domain boundary. The films are in fact annealed at 1000–1300 K in UHV, which corresponds to rather reducing conditions. Additionally, kinetics disfavor the dissociation of oxygen once the surface is oxidized.

Although the adsorption site of the O atom in Fig. 3(b) behaves like a defect, we should note that it is not a localized structural defect. Without the additional oxygen atom, each O_s atom has 5 or 6 oxygen nearest neighbors in plane and binds to 3 Al_s atoms, just like in the unperturbed oxide. Also the coordination of all other atoms cannot be distinguished from the perfect oxide film. The additional O atom in Fig. 3(b) violates some of these rules but still cures the electronic defect.

Our model for the antiphase domain boundary favors metal adsorption at the domain boundary compared to the perfect oxide film. We have determined that adsorption of single Au, Pd, and Rh atoms is more favorable at the boundary by 0.3, 0.7, and 1.7 eV than above the most favorable site on the perfect film. For Pd, it has been shown that antiphase domain boundaries are in fact preferentially occupied at higher temperatures [8]. However, for a complete understanding, the kinetics, in particular, diffusion barriers, need to be considered as well.

In summary, in the present work we have derived a model for antiphase domain boundaries of the ultrathin alumina film on NiAl(110). The final stoichiometry of the proposed model as well as the calculated electronic properties indicate that its structure is O deficient. Hence, two Al $3p$ electrons fail to find the corresponding empty O $2p$ conduction band states. An insulating surface layer is restored by transferring these electrons to the metallic NiAl support, which acts as an electron reservoir. A counteracting field develops, causing a local band bending and a shift of the valence and conduction bands to lower energies. The oxygen-deficient domain boundary thus behaves like a native electron donor, which is a much disputed behavior for oxygen-deficient defects in transition metal oxides, such as ZnO or high-k gateoxides (see, e.g., Refs. [21,22]). The present work is the first atomic-scale observation of such a center on a wide-band-gap oxide accompanied by careful DFT calculations. A further intriguing observation is the existence of this electronic defect despite the fact that the building principles of the perfect film are maintained. The commonly assumed one-to-one correspondence between *structural* and *electronic* defects is thus violated. Furthermore, a favorable adsorption center at the domain boundary is identified. We believe that the existence of such sites is universal to metal-oxide interfaces and domain boundaries, and is thus relevant for diverse research fields, such as semiconductor physics or heterogeneous catalysis (see also Ref. [23]).

This work was supported by the Austrian *Fonds zur Förderung der wissenschaftlichen Forschung* and the European Union under Contract No. NMT-CT-2004-001594 (project "GSOMEN"). M. K. is grateful to the Studienstiftung des deutschen Volkes for financial support.

*Corresponding author.
Electronic address: georg.kresse@univie.ac.at

[1] E. Wahlström *et al.*, Phys. Rev. Lett. **90**, 026101 (2003).
[2] M. Bäumer and H.-J. Freund, Prog. Surf. Sci. **61**, 127 (1999).
[3] M. Kulawik, N. Nilius, H.-P. Rust, and H.-J. Freund, Phys. Rev. Lett. **91**, 256101 (2003).
[4] N. Nilius, M. Kulawik, H.-P. Rust, and H.-J. Freund, Phys. Rev. B **69**, 121401(R) (2004).
[5] R. M. Jaeger *et al.*, Surf. Sci. **259**, 235 (1991).
[6] J. Libuda *et al.*, Surf. Sci. **318**, 61 (1994).
[7] A. Stierle *et al.*, Science **303**, 1652 (2004).
[8] N. Nilius, T. M. Wallis, and W. Ho, Phys. Rev. Lett. **90**, 046808 (2003).
[9] G. Kresse *et al.*, Science **308**, 1440 (2005).
[10] H.-P. Rust, J. Buisset, E. K. Schweizer, and L. Cramer, Rev. Sci. Instrum. **68**, 129 (1997).
[11] A. Stierle, F. Renner, R. Streitel, and H. Dosch, Phys. Rev. B **64**, 165413 (2001).
[12] G. Kresse and J. Furthmüller, Comput. Mater. Sci. **6**, 15 (1996).
[13] J. P. Perdew *et al.*, Phys. Rev. B **46**, 6671 (1992).
[14] J. Heyd, G. E. Scuseria, and M. Ernzerhof, J. Chem. Phys. **118**, 8207 (2003).
[15] J. Paier, R. Hirsch, M. Marsman, and G. Kresse, J. Chem. Phys. **122**, 234102 (2005).
[16] P. E. Blöchl, Phys. Rev. B **50**, 17 953 (1994).
[17] G. Kresse and D. Joubert, Phys. Rev. B **59**, 1758 (1999).
[18] J. Tersoff and D. R. Hamann, Phys. Rev. B **31**, 805 (1985).
[19] M. Hagen and M. W. Finnis, Philos. Mag. A **77**, 447 (1998).
[20] S. Andersson *et al.*, Surf. Sci. **442**, L964 (1999).
[21] A. Janotti and C. G. Van de Walle, Appl. Phys. Lett. **87**, 122102 (2005).
[22] A. Kerber *et al.*, IEEE Electron Device Lett. **24**, 87 (2003).
[23] B. Hammer, Top. Catal. **37**, 3 (2006).